Theor Chem Acc (2001) 106:352–363
DOI 10.1007/s002140100284

Theoretical
Chemistry Accounts

Regular article

Theoretical investigation into structures and magnetic properties of smaller fullerenes and their heteroanalogues

Zhongfang Chen[1,2], **Haijun Jiao**[1,3], **Michael Bühl**[2], **Andreas Hirsch**[1], **Walter Thiel**[2]

[1] Institut für Organische Chemie, Universität Erlangen-Nürnberg, Henkestrasse 42, 91054 Erlangen, Germany
[2] Max-Planck-Institut für Kohlenforschung, Kaiser-Wilhelm-Platz 1, 45470 Mülheim an der Ruhr, Germany
[3] Laboratoire de Chimie du Solide et Inorganique Moléculaire, UMR CNRS 6511, Université de Rennes 1, 35042 Rennes Cedex, France

Received: 26 March 2001 / Accepted: 10 May 2001 / Published online: 11 October 2001

Abstract. The smaller fullerenes, C_{20}, C_{24}, C_{28}, C_{32}, C_{36}, C_{40} and C_{50}, their hydrogenation products and selected B-, N- and P-doped analogues have been investigated systematically at the B3LYP/6-31G* density functional level of theory. The degree of spherical electron delocalization is evaluated by using the computed nucleus-independent chemical shifts (NICS) at the cage center and the individual ring centers of interest. The calculated NMR chemical shifts and the NICS values at the cage center, which can be accessed by endohedral ^{3}He chemical shifts, should provide a basis for further experimental characterization of these compounds.

Key words: Smaller fullerenes – Aromaticity – Nucleus-independent chemical shifts – Endohedral helium chemical shifts

1 Introduction

Are there fullerenes smaller than C_{60} which are stable enough to be isolated? The first such claim was made by Piskoti et al. [1], but the nature of their isolated compound formulated as C_{36} is still unclear. In the gas phase, a number of fullerenes C_n ($60 > n \geq 20$ [2]) have been detected with mass spectroscopic methods.

Numerous theoretical calculations have been performed for smaller fullerenes. For C_n clusters with $n < 20$, no fullerene structures are possible and the most stable isomers are usually chainlike or monocyclic [3–8]. For C_{20}, the most stable isomer can have a ring, a bowl or a fullerene structure, depending on the computational method employed [9]. Experimentally, each of these C_{20} isomers can be produced under suitable reaction conditions [2, 10], for example, C_{20} fullerene from its perhydrogenated form, dodecahedrane, $C_{20}H_{20}$ [2]. Similar alternatives exist for C_{24} [11–15], where the latest calculations indicate the fullerene form (D_6) as the most stable one [15].

The next member of the smaller fullerenes is C_{28}, originally proposed in 1987 [16]. The T_d isomer is most stable at the self-consistent-field (SCF) level [17]. Density functional calculations confirmed the quintet ground state of C_{28} [18], which is further supported by recent computations on 24 structures at various levels of theory [19]. The observation of species $M@C_{28}^+$ (M = Ti, Zr, Hf, U) in a mass spectrometer strongly suggests the existence of endohedral structures $M@C_{28}$ [17], and a theoretical study of a variety of $M@C_{28}$ species has also been reported [20].

Under appropriate conditions, C_{32} was found to be the most stable fullerene below C_{60} [21]. The hydrogen adduct $C_{32}H_2$ (D_{3d}) is expected to be relatively stable because its remaining 15 double bonds are contained within three naphthalene subunits and strain is released at the two carbon atoms lying on the C_3 axis [22, 23].

Of much current interest is C_{36} fullerene chemistry, including, for example, the proposed macroscopic solid-state synthesis [1], the possible dimer in a monolayer [24] and its hydrides and oxyhydrides [25, 26]. A series of theoretical studies on the structure and bonding [27–35] of C_{36} and its charged species [36] have been reported. Both ab initio and density functional theory (DFT) data show that the most stable isomer of C_{36} has a D_{6h} triplet ground state [31, 37]. Most recently, the structures and aromaticity of both neutral and charged C_{36} species, their hydrogen adducts and B- and N-doped analogues have been evaluated [38].

The D_2 and D_{5d} isomers are the two most stable structures for C_{40} [39]. Although not very stable [23, 40, 41], C_{40} can have an open-shell ground state, which leads to extraordinary thermodynamic stability for its T_d symmetrical derivatives such as $C_{40}H_4$ and $C_{36}N_4$ [42].

Correspondence to: andreas.hirsch@organik.uni-erlangen.de, thiel@mpi-muelheim.mpg.de

Fullerene C_{50} has been less studied theoretically though it also belongs to the "magic peaks" in some experiments [21]. The D_{5h} isomer is aromatic and shows strong electron delocalization [43, 44].

Besides the pure carbon cages, their adducts have also gained great interest [21, 45–48] with consideration of their so-called "hidden" valence [22, 49, 50]. The surface doping by heteroatoms such as boron and nitrogen [46, 47, 51–53] and the isoelectronic structure of C_{24} – boron nitride $B_{12}N_{12}$ [54] – have also been investigated.

Numerous theoretical studies were devoted to the magnetic properties of C_{60} and higher fullerenes [43, 44, 55–61], but only some of the smaller fullerenes have also been covered so far [38, 43, 44]. To aid further synthesis and characterization of these compounds, we performed systematic DFT computations on the smaller fullerenes, their doped analogues and hydrogen adducts mentioned previously. The aromaticity (degree of electron delocalization) is evaluated by using the computed nucleus-independent chemical shifts (NICS) [62] at the cage center and the individual ring centers of interest. The NICS is a useful criterion for the aromaticity of a molecule [44, 62], and the NICS at the cage center has essentially the same value as the ^{3}He endohedral shift, which is a valuable experimental tool for characterizing fullerenes and their derivatives [55, 63, 64]. Ab initio and DFT calculated NMR chemical shifts for ^{13}C and other relevant nuclei are also reported. In addition, the interaction between the endohedral helium atom and the cages is considered.

2 Computational methods

The geometries were fully optimized in the given symmetry at the B3LYP/6-31G* density functional level of theory [65] by using the Gaussian 98 program [66]. The NICS [62] values of both the cage centers and the individual ring centers of interest were computed at both the GIAO-SCF/6-31G* and B3LYP/6-31G* levels with the B3LYP/6-31G* geometries. ^{13}C and ^{1}H chemical shifts were calculated relative to benzene and converted to the tetramethylsilane scale using the experimental values for benzene ($\delta = 128.5$ for C and 7.3 for H). ^{31}P chemical shifts were computed relative to H_3PO_4 and converted to the usual phosphate scale using the experimental value ($\delta = 328.4$ ppm) [67]. ^{11}B chemical shifts were calculated relative to B_2H_6 and converted to the usual $BF_3.O(C_2H_5)_2$ scale using the experimental $\delta(^{11}B)$ value of 16.6 ppm for B_2H_6 (cf. the procedure outlined in Ref. [68]). ^{15}N chemical shifts are reported directly relative to NH_3 at the same level.

In addition, the NICS values were computed for a C_{36} isomer with the GIAO-MP2 method [69] in its direct implementation [70], employing a contracted [4s2p1d] Huzinaga basis [71], denoted DZP (d exponent: 0.8), and a RI-MP2/6-31G* optimized geometry (i.e. using a very cost efficient approximation to the MP2 method, termed resolution of identity [72], together with the 6-31G* basis and a suitable 8s5p3d1f auxiliary basis set [73, 74]). These calculations were performed with the TURBOMOLE suite of programs [75]. For comparison, GIAO-DFT computations were performed for C_{36} using the same geometry and basis set, together with the B3LYP and BPW91 combinations of density functionals, the latter comprising Becke's 1988 exchange [76] and Perdew and Wang's 1991 correlation functional [77, 78].

The total energies and the HOMO–LUMO gap energies for all the species studied here are summarized in Table 1. For the discussion of local and global aromaticity of the species studied, the NICS values calculated at the GIAO-SCF/6-31G* level are employed first.

3 Results and discussion

3.1. Geometries, local and global aromaticity

3.1.1 C_{20} series

Owing to Jahn–Teller distortion, the singlet ground state of C_{20} has C_2 instead of I_h symmetry, and this is confirmed by frequency analysis; the C–C bond lengths vary from 1.405 to 1.517 Å, indicating a pronounced degree of electron delocalization (Fig. 1). Indeed, the five-membered rings are aromatic with NICS values of −4.9 and −17.0 ppm, while the cage center has an even more negative NICS value of −36.7 ppm. Double oxidation results in C_{20}^{2+}, which has a closed-shell singlet ground state in I_h symmetry and is highly aromatic with NICS values of −30.8 and −73.1 ppm at the centers of the five-membered rings and the cage, respectively. This huge difference between C_{20} and C_{20}^{2+} is ascribed to the completely filled valence shell with $2(N+1)^2$ electrons ($N = 2$) and reflects the perfect spherical aromaticity in C_{20}^{2+} [79].

Complete hydrogenation of C_{20} leads to dodecahedrane ($C_{20}H_{20}$), which represents a normal saturated hydrocarbon with C–C bond lengths of 1.557 Å and a NICS value of −0.8 ppm at the cage center, comparable to the value (−1.1 ppm) for adamantane [62].

3.1.2 C_{24} series

The structure of C_{24} (D_6) can be considered as a [12]trannulene [80] capped with two benzene rings at

Table 1. B3LYP/6-31G* total energies and HOMO–LUMO gaps

Species	Symmetry	Energy (au)	Gap (eV)
C_{20}	C_2	−761.4443	1.95
C_{20}^{2+}	T_d	−760.7802	3.91
$C_{20}H_{20}$	I_h	−774.1850	8.00
C_{24}	D_6	−913.8400	0.76
$C_{24}H_{12}$	D_{6d}	−921.6280	5.49
$C_{24}H_{12}$	D_6	−921.4190	1.94
$C_6B_9N_9$	C_3	−945.2565	2.51
C_{28} (quintet)	T_d	−1,066.3373	4.20
C_{28}^{4-}	T_d	−1,065.7916	3.99
$C_{24}N_4$	T_d	−1,133.0600	4.41
$C_{24}B_4$	T_d	−1,013.4170	2.79
$C_{24}P_4$	T_d	−2,279.4789	3.09
$C_{28}H_4$	T_d	−1,068.9162	3.32
C_{32}	D_3	−1,218.8329	2.60
$C_{32}H_2$	D_3	−1,220.1051	2.94
C_{32}	D_{3d}	−1,218.7151	1.60
$C_{32}H_2$	D_{3d}	−1,219.9771	1.40
C_{36} (singlet)	D_{6h}	−1,371.2569	1.10
C_{36} (triplet)	D_{6h}	−1,371.2630	1.80
C_{36}	D_{2d}	−1,371.2624	1.39
C_{36}	C_{2v}	−1,371.2506	1.53
C_{40}	D_2	−1,523.7283	2.00
C_{40}	D_{5d}	−1,523.7114	2.15
C_{40}^{4-}	T_d	−1,523.2604	2.49
$C_{36}N_4$	T_d	−1,590.4248	3.12
$C_{36}B_4$	T_d	−1,470.6308	1.04
$C_{36}P_4$	T_d	−2,736.7253	2.15
$C_{40}H_4$	T_d	−1,526.2167	2.42
C_{50}	D_{5h}	−1,904.9231	1.28

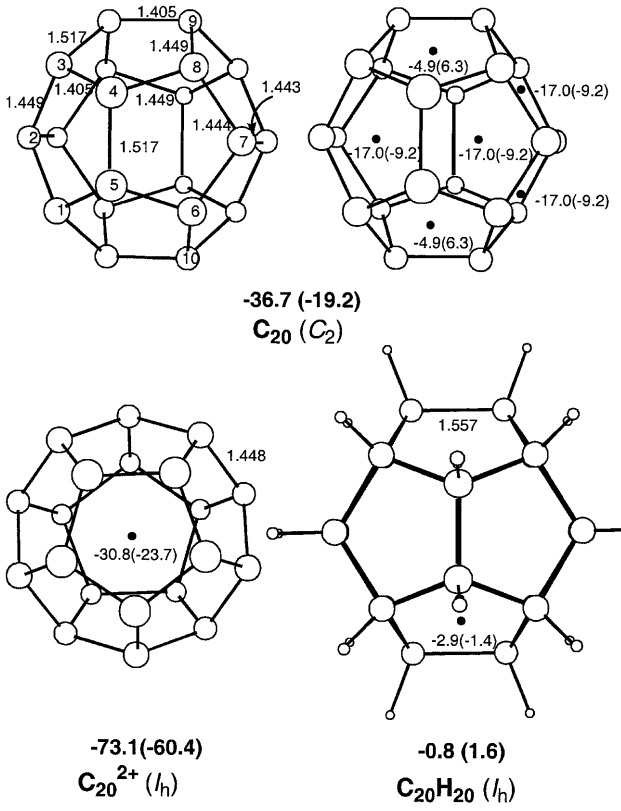

Fig. 1. B3LYP/6-31G* bond lengths (angstroms) and nucleus-independent chemical shift (*NICS*) values (parts per million) from GIAO-SCF/6-31G* (B3LYP/6-31G* in *parentheses*). The NICS values at the cage centers are given in *bold* below each structure, while those at individual ring centers are shown in the corresponding ring

both sides (Fig. 2). Apart from the unique C–C bond length of the six-membered rings (1.423 Å), the central [12]trannulene ring has localized C–C bond lengths of 1.365 and 1.463 Å, while the C–C bond lengths between the six-membered rings and the [12]trannulene ring are 1.531 Å. In accord with these geometric properties, the NICS value at the center of the six-membered ring of −6.9 ppm is reduced compared to the benzene value (−11.5 ppm), and the NICS value at the cage center of 15.6 ppm is also smaller compared to the [12]trannulene value (35.7 ppm). This is due to the compensation of local diatropic and paratropic ring currents.

With partially hydrogenated $C_{24}H_{12}$, this compensation effect can be assessed by the difference between hydrogenation of the [12]trannulene subunit and the two six-membered rings. In the former case (D_{6d}), the [12]trannulene ring becomes saturated and the NICS value and the C–C bond length of the six-membered ring are benzene-like (−13.4 ppm versus 1.399 Å). The NICS value of −18.0 ppm at the cage center can be considered essentially as the sum of the two separated benzene rings since the NICS value at the point 1.64 Å above the benzene ring center is −8.0 ppm [62]. In the other case (D_6), hydrogenation saturates the two six-membered rings, and the antiaromatic property of [12]trannulene is clearly shown by the NICS value of 11.6 ppm at the cage center. The D_{6d} species with sat-

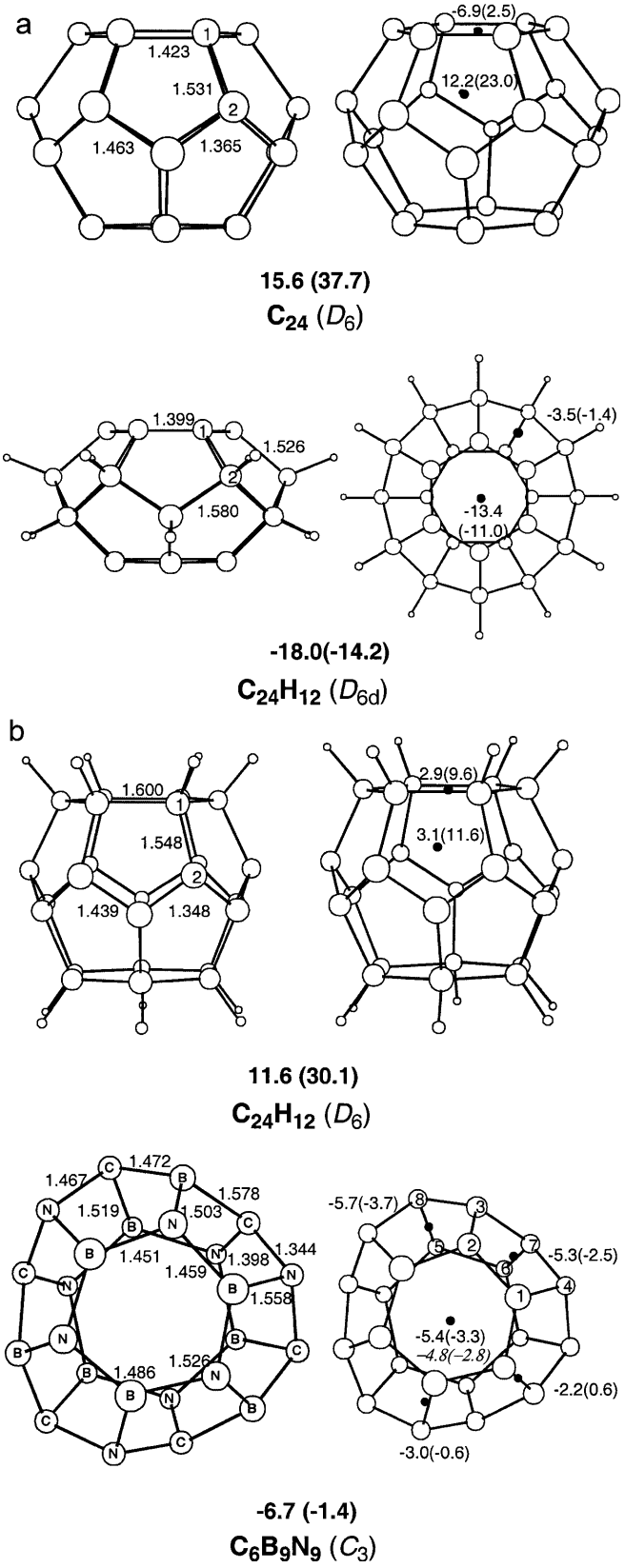

Fig. 2. B3LYP/6-31G* bond lengths (angstroms) and NICS values (parts per million) from GIAO-SCF/6-31G* (B3LYP/6-31G* in *parentheses*). The NICS values at the cage centers are given in *bold* below each structure, while those at individual ring centers are shown in the corresponding ring

urated [12]trannulene is 131 kcal/mol more stable than the D_6 species with saturated benzene rings. This is due to the combined effect of the reduced strain in the central belt region and aromaticity: in the D_{6d} form, the aromatic benzene rings are maintained and the antiaromatic trannulene ring is hydrogenated, while the opposite is true for the D_6 form.

In the BN-doped analogue $C_6B_9N_9$ (C_3) with two borazine rings, all the local rings and the cage have only small NICS values and they can thus be considered to be nonaromatic. The high degree of electron localization on the nitrogen center in borazine [81] is also reflected in this molecule.

3.1.3 C_{28} series

As shown in Fig. 3, the T_d symmetrical C_{28} structure contains four separated six-membered rings connected by four carbon atoms at each vertex of a tetrahedron. As a consequence of this high symmetry, C_{28} has a quintet ground state, and the valence orbitals are half filled [17–19]. Both the six- and five-membered rings have only moderate NICS values (−7.1 versus −5.3 ppm), while the NICS value at the cage center is somewhat more pronounced (−13.0 ppm). With an additional four electrons (C_{28}^{4-}), the situation changes dramatically, since the valence shells are now completely filled. Not only the NICS at the hexagon (−21.9 ppm) and pentagon (−13.4 ppm), but also that at the cage center (−35.5 ppm) becomes more negative than those in the neutral case; therefore the tetraanion is more aromatic, even though there are no large geometric changes. This is again due to the complete filling of the valence orbitals, and (C_{28}^{4-}) in T_d symmetry follows the $2(N+1)^2$ rule for maximal aromaticity in spherical cages ($N = 3$) [79].

A highly negative NICS value (−30.9 ppm) is also found for the T_d symmetrical $C_{24}N_4$, which is isoelectronic with C_{28}^{4-} and also follows the $2(N+1)^2$ rule for maximal spherical aromaticity. This suggests a high delocalization of the electrons rather than isolated electron lone pairs at the nitrogen atoms. In contrast to $C_{24}N_4$, the valence isoelectronic $C_{24}P_4$ is quite different. For example, the six-membered ring in $C_{24}P_4$ has a similar NICS value (−5.9 ppm) as C_{28}, whereas the five-membered ring in $C_{24}P_4$ has a positive NICS value (4.5 ppm). The NICS value of 1.3 ppm at the cage center reveals $C_{24}P_4$ to be nonaromatic, indicating localization of the

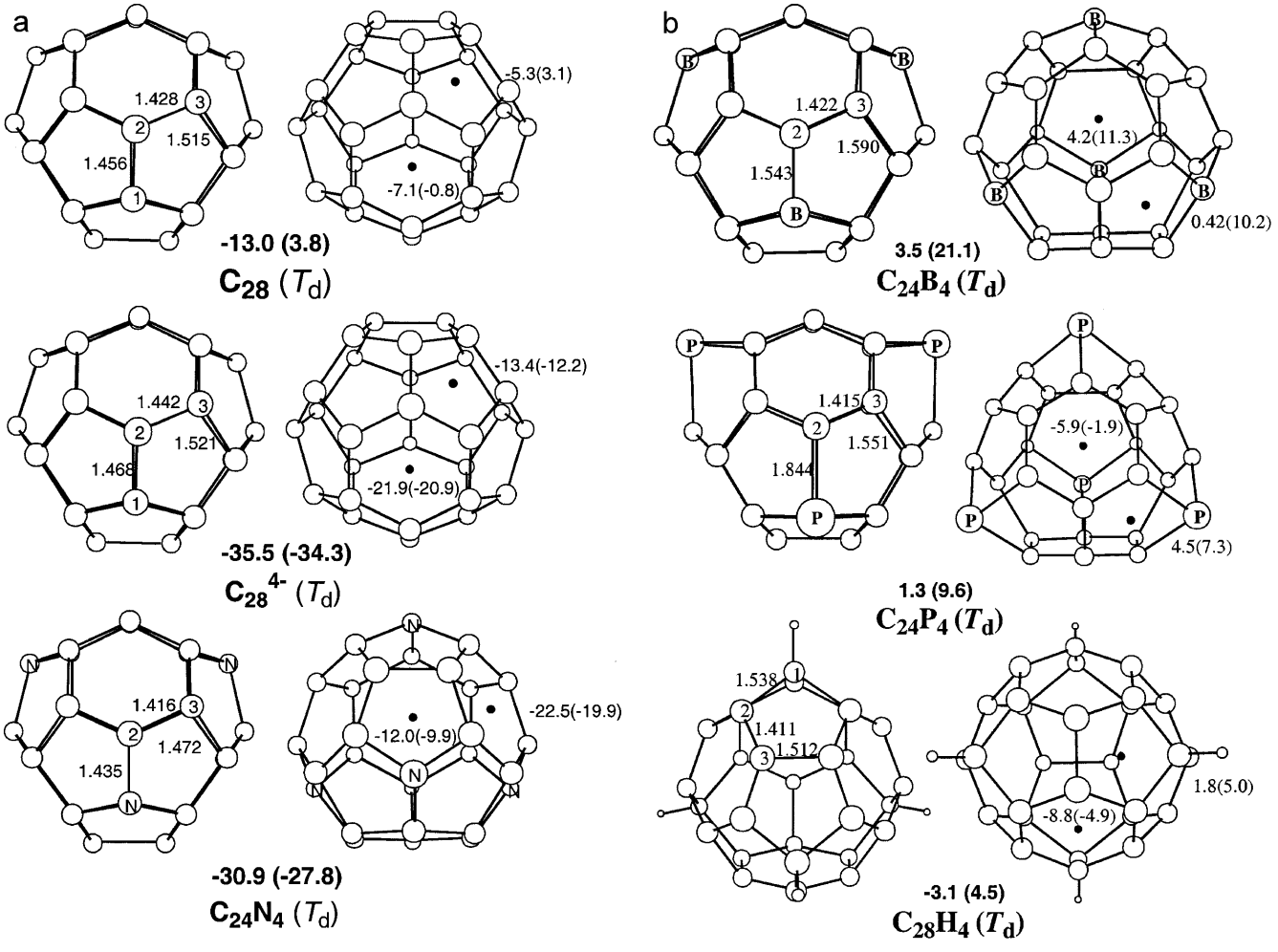

Fig. 3. B3LYP/6-31G* bond lengths (angstroms) and NICS values (parts per million) from GIAO-SCF/6-31G* (B3LYP/6-31G* in *parentheses*). The NICS values at the cage centers are given in *bold* below each structure, while those at individual ring centers are shown in the corresponding ring

phosphorous lone pairs. Owing to the incomplete filling of the valence orbitals in T_d symmetry, $C_{24}B_4$ and the tetrahydrogenated $C_{28}H_4$ are also nonaromatic, with NICS values of 3.5 and −3.1 ppm at the cage centers, respectively.

3.1.4 C_{32} series

Among the two structural isomers considered for the C_{32} fullerene, the D_3 one is more stable than the D_{3d} one by 73.9 kcal/mol. There are six independent carbon atoms and three unique ring centers in the D_3 structure (Fig. 4). The negative NICS values indicate that both the five- and the six-membered rings exhibit strong diatropic currents, resulting in a very large endohedral shielding of −53.2 ppm, in good agreement with computed value of −52.7 ppm at the GIAO-SCF/DZP//BP86/3-21G level [44]. This large NICS value has, in part, been ascribed to the radial dependence of ring current effects [43], and we note, in addition, that C_{32} fulfills the $2(N+1)^2$ rule for spherical aromaticity [79]. The cigar-shaped D_{3d} isomer has a less negative NICS value (−39.3 ppm) and is thus less aromatic than the more stable and more spherical D_3 structure.

Upon hydrogenation along the C_3 axis of these two isomers ($C_{32}H_2$), the D_3 form remains more stable than the D_{3d} form (by 80.3 kcal/ mol), but the former now has a much less negative NICS value (−32.7 ppm) than the latter (−63.0 ppm).

3.1.5 C_{36} series

At the B3LYP/6-31G* level, the triplet D_{6h} ground state is separated only slightly from the next singlet D_{2d} state. In the D_{6h} structure, there are only three independent carbon atoms and four independent carbon–carbon bonds. As shown in Fig. 5, there are no significant geometrical differences between the singlet and the triplet states. The six- and five-membered rings are aromatic in both states, and the less stable singlet ($^1A_{1g}$ state, HOMO b_{2u}, LUMO b_{1g}) is more aromatic than the triplet ($^3A_{2u}$ state, SOMOs b_{2u} and b_{1g}) according to the computed NICS values at the cage centers (−38.2 versus −27.1 ppm, respectively).

In addition, we calculated two other singlet states (D_{2d} and C_{2v}) (Fig. 5). The former is nearly isoenergetic with the D_{6h} triplet ground state, whereas the C_{2v} structure is less stable than the ground state by 7.8 kcal/mol. Both the D_{2d} and the C_{2v} singlet states (NICS = −15.4 and

Fig. 4. B3LYP/6-31G* bond lengths (angstroms) and NICS values (parts per million) from GIAO-SCF/6-31G* (B3LYP/6-31G* in *parentheses*). The NICS values at the cage centers are given in *bold* below each structure, while those at individual ring centers are shown in the corresponding ring

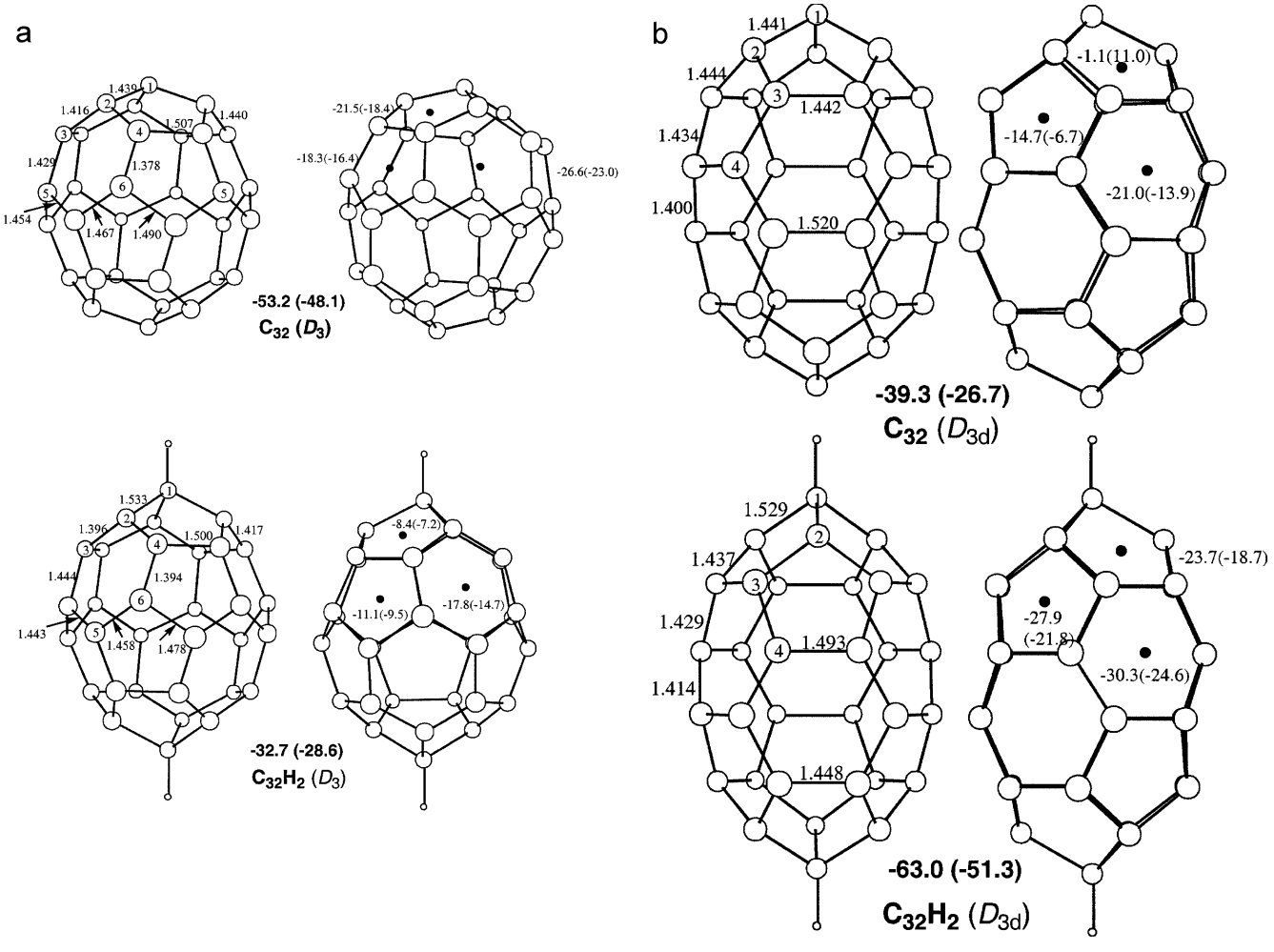

−17.6 ppm) are less aromatic than the two D_{6h} isomers, respectively.

3.1.6 C_{40} series

Among the two isomers considered for the C_{40} fullerene, the D_2 form is predicted to be the ground state [39], which is 10.6 kcal/mol more stable than the D_{5d} form at the B3LYP/6-31G* level. As shown in Fig. 6, the D_2 isomer has six types of rings: four are antiaromatic or nonaromatic five-membered rings and two are moderately aromatic six-membered rings. The entire cage exhibits global nonaromatic character with a NICS value of 4.0 ppm at the cage center.

On the other hand, the less stable D_{5d} isomer with three types of rings can be considered as two fused corannulene-like caps, which are the standard components of C_{60} and C_{70}. The central pentagons of the caps show strong paratropic currents, while the hexagons have only very weak or nondiatropic currents. The pentagons in the belt also exhibit moderate antiaromatic character. Thus the whole system is nonaromatic, with a NICS value of 2.8 ppm.

The T_d isomer of C_{40} should have an open-shell ground state (two electrons in the t_2 HOMO) and should thus be very reactive [42], but the perfect T_d symmetry must be lowered because of first-order Jahn–Teller distortion [82]. However, its ions, adducts and doped analogues may be stable. The tetraanion C_{40}^{4-}, its doped analogues and the hydrogen adduct $C_{40}H_4$ adopt T_d structures containing 12 pentagons and ten hexagons, and there are three types of symmetry-equivalent atoms in the cages, including the four C1/*X*-type atoms (X = B, N, P, CH) in the vertices of a tetrahedron, each being the triplet vertex of pentagons, and the twelve C2-type atoms connecting directly to the C1-type atoms.

There are three types of rings in T_d symmetry, one five-membered ring and two six-membered rings. The six-membered rings with two C2-type carbons have a boatlike conformation and exhibit significant aromatic character (NICS values in the range −9 to −16, except for −2.6 for $C_{36}B_4$), while the other six-membered rings built by the C3-type carbon atoms are nearly coplanar and are less aromatic (NICS values from −0.5 to 0.2). The five-membered rings are aromatic for C_{40}^{4-} and $C_{36}N_4$, but are antiaromatic for the other species. As a whole, the electron-rich C_{40}^{4-} and $C_{36}N_4$ exhibit marked aromaticity (NICS −15.7 and −11.8, respectively), while $C_{36}P_4$, $C_{40}H_4$ and $C_{36}B_4$ are nonaromatic (NICS −3.5, −3.6 and 1.3 ppm at the cage centers, respectively).

3.1.7 C_{50} series

The optimized structure of C_{50} with D_{5h} symmetry and the NICS values are shown in Fig. 7. Both the five-membered and the six-membered rings are aromatic,

►

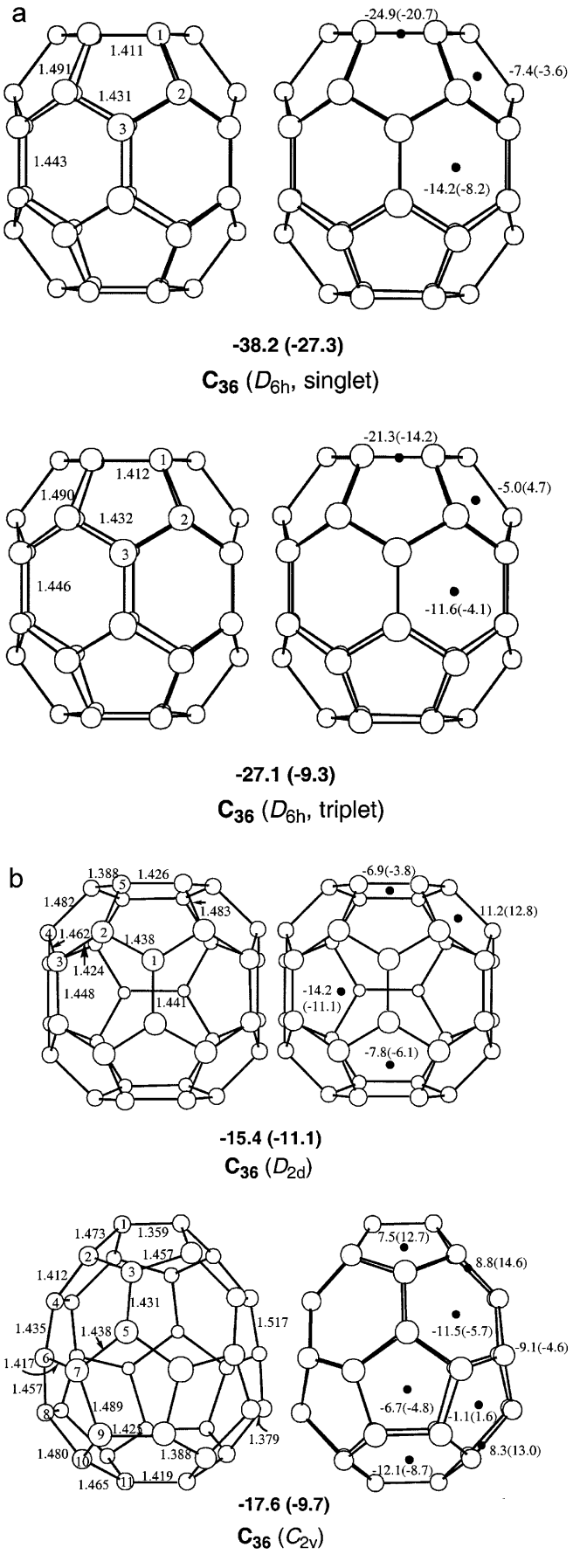

Fig. 5. B3LYP/6-31G* bond lengths (angstroms) and NICS values (parts per million) from GIAO-SCF/6-31G* (B3LYP/6-31G* in *parentheses*). The NICS values at the cage centers are given in *bold* below each structure, while those at individual ring centers are shown in the corresponding ring

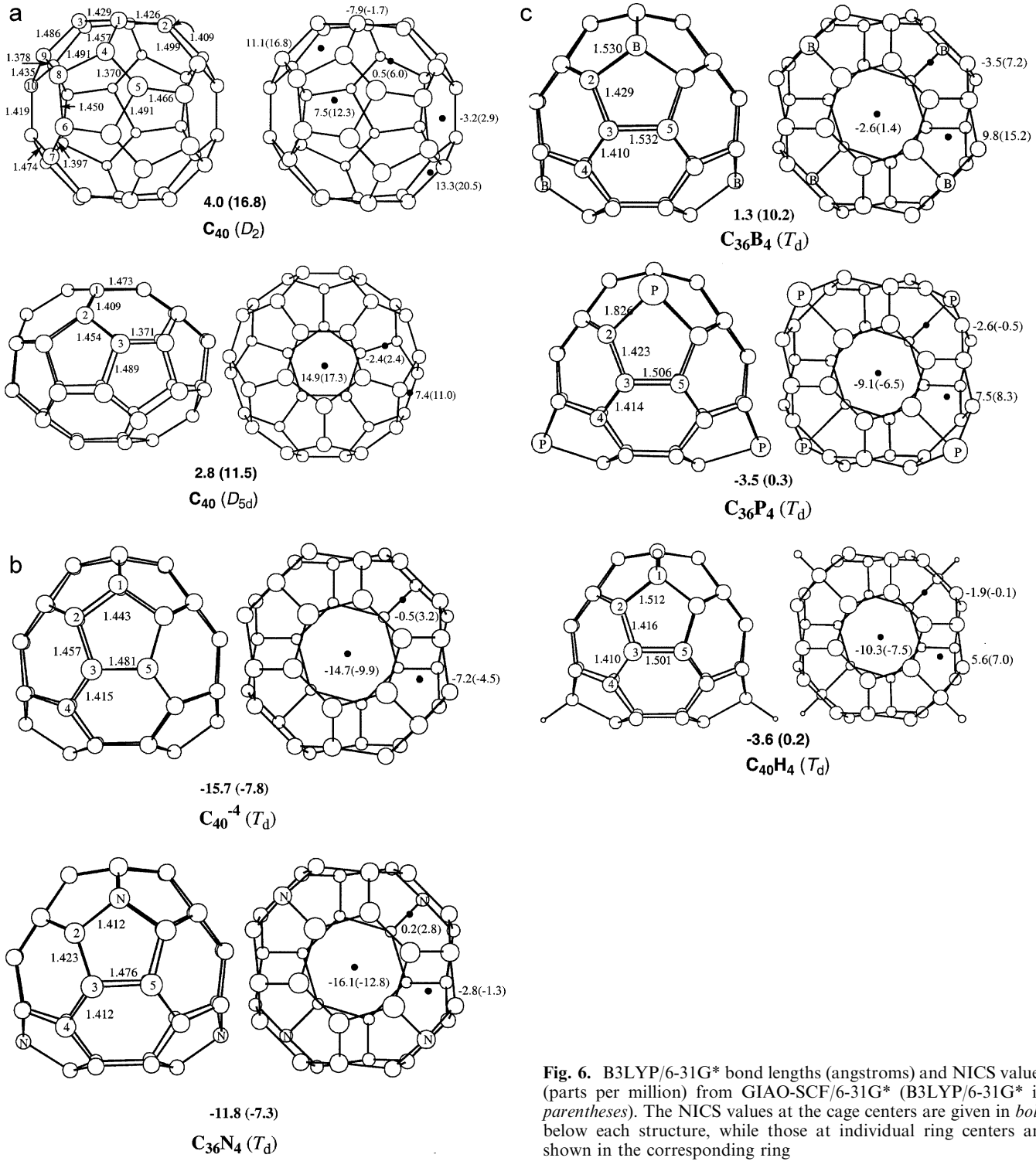

Fig. 6. B3LYP/6-31G* bond lengths (angstroms) and NICS values (parts per million) from GIAO-SCF/6-31G* (B3LYP/6-31G* in *parentheses*). The NICS values at the cage centers are given in *bold* below each structure, while those at individual ring centers are shown in the corresponding ring

with NICS values between −7.5 and −18.2 ppm. Likewise, as a whole, the cage has highly aromatic character (NICS −37.1 ppm) and thus serves as another example of the $2(N+1)^2$ rule of spherical aromaticity [79]. The C_{50} (D_{5h}) structure can be built by inserting a C_{10} belt into C_{40} (D_{5d}), in the same way as C_{70} is constructed from C_{60}. It is interesting to note that the [0_5] paracyclophane belt as a fragment in C_{50} is well delocalized, the C–C bond (1.402 Å) connecting the phenyl rings and the C–C bond (1.390 Å) in the equatorial hexagons are in the aromatic range, so the belt has considerable benzenoid character. The equatorial six-membered rings are aromatic with a NICS value of −11.1, and thus provide a remarkable contribution to the high aromaticity of the whole cage structure; this resembles C_{70} closely. However, the fragment differs from the free [0_5]

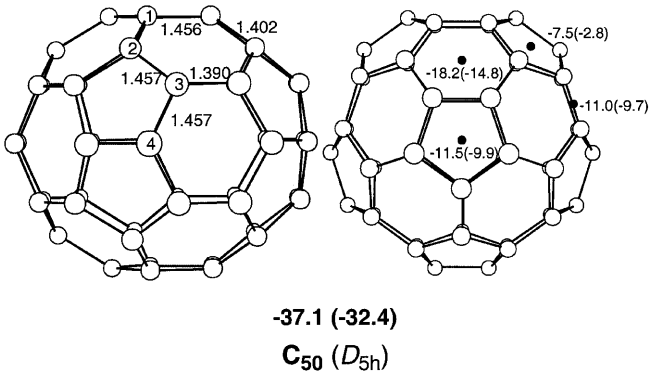

Fig. 7. B3LYP/6-31G* bond lengths (angstroms) and NICS values (parts per million) from GIAO-SCF/6-31G* (B3LYP/6-31G* in *parentheses*). The NICS values at the cage centers are given in *bold* below each structure, while those at individual ring centers are shown in the corresponding ring

paracyclophane belt, which is essentially a quinonoid form, with nonaromatic, six-membered rings [83].

3.2 The accommodation energy of endohedral helium as a guest

Would a helium atom still fit into the smaller fullerenes and their derivatives and could it be incorporated in such amounts to be detected with ^{3}He NMR spectroscopy? Recently a helium atom was put into $C_{20}H_{20}$ by helium ion bombardment [84]. The accommodation energy was computed to be 35.0 kcal/mol (1.52 eV) at the B3LYP/6-31G* level. Similar values, 33.0 (1.43 eV, this work) and 33.8 kcal/mol [85], have been obtained at the counterpoise-corrected MP2/6-31G* level (employing the 6-31G** basis for He) and the MP2(FC)/6-311G(d, p) level of theory, respectively. The computationally less demanding B3LYP approach is thus apparently well suited to describe the repulsive van der Waals interaction. Since there are 30 C–C single bonds in $C_{20}H_{20}$, the accommodation energy for each C–C bond is less than 1.2 kcal/mol. Note also that the mean bond enthalpy of a C–C single bond is 83.2 kcal/mol [86]; therefore, it is clear that once implanted He will remain trapped inside the cage.

In order to test if the same can be expected for other small fullerenes, the corresponding endohedral helium complexes He@C_n were optimized at the B3LYP/6-31G* level. He encapsulation elongates the C–C bonds only slightly (progressively less with increasing cage size), and no large geometric changes occur. The computed accommodation energies (in electron volts) are 3.29 for C_{20}, 1.73 for C_{24}, 0.89 for C_{28}, 0.38 for C_{36}, 0.18 for C_{40} and 0.06 for C_{50}. Except for C_{20}, these energies are relatively small, and they decrease with increasing cage size. Inclusion of dispersion effects would probably result in a net binding of He in C_{50}. It is worth noting that all noble gases are computed to be bound inside C_{60} at the counterpoise-corrected MP2 level [87]. Thus, under suitable experimental conditions, isolation of these endohedral species might prove possible. By analogy, the same should be true for exohedrally or cage-modified derivatives.

3.3 Theoretical NMR spectra of the smaller fullerenes and their doped analogues

^{13}C NMR plays a major role in the structural characterization of the fullerenes and their derivatives. In order to assist in further spectroscopic studies, we report ab initio and DFT-calculated ^{13}C, ^{1}H, ^{15}N, ^{11}B and ^{31}P NMR chemical shifts for the singlet-state species studied here (Table 2). In most cases, the SCF- and the DFT-computed δ values agree very well. While nearly all species in this series have not been identified yet, we expect that these calculated NMR spectra may be helpful once they are synthesized and isolated.

3.4 The performance of density functional methods for calculations of endohedral chemical shifts of fullerenes

At present, the experimental ^{3}He NMR chemical shifts of fullerenes and their derivatives can be reproduced reasonably well (within about 2–3 ppm) by theoretical calculations at the Hartree–Fock (HF)-GIAO level; somewhat larger errors occur with highly charged anions. In most of the cases studied so far, the use of the GIAO-DFT method has improved the accord between theory and experiment. C_{60} is a spectacular exception, however, since the B3LYP hybrid functional affords an endohedral shift of 1.0 ppm (BPW91 1.5 ppm), i.e., a substantial deshielding of 10 ppm with respect to the HF-GIAO method, and a large discrepancy to experiment, −6.3 ppm [63]. The individual ring currents in C_{60} have much more paratropic character at the DFT level, and the diatropic currents in the six-membered rings have practically vanished at this level [88]. How will electron correlation affect the ring currents in the smaller fullerenes? Is there some general trend for the computed endohedral chemical shifts for the DFT method?

In order to compare GIAO-SCF and GIAO-DFT results with electron-correlated ab initio data, we computed NICS values for the D_{6h} singlet state of C_{36} at the GIAO-MP2 level (Table 3). These computations employed a slightly different geometry (RI-MP2/6-31G*) and a slightly larger basis set (DZP) than used in the other calculations reported here, but this does not affect the assessment of the various theoretical methods. Interestingly, all the electron-correlated methods, i.e., DFT and MP2, afford very similar NICS values, within a few parts per million of each other for the different positions. The close similarity between the B3LYP and MP2 data is particularly noteworthy (last two columns in Table 2). For the NICS values of the cage pentagons and hexagons, a deshielding of a few parts per million is computed on going from SCF to DFT or MP2, adding up to a notable 12–15 ppm downfield shift for the endohedral NICS value. Since the B3LYP data account for a good portion of electron correlation, they should, in principle, be more accurate than the corresponding SCF values.

Table 2. Calculated NMR chemical shifts (parts per million). The numbering system is given in Figs. 1–7

Species	Symmetry	Atom	Hartree–Fock[a]	B3LYP[b]
C_{20}	C_2	C1	198.4	191.5
		C2, C3[c]	180.3	165.4
		C4	183.5	189.2
		C5, C6[c]	180.1	165.1
		C7, C8[c]	198.9	191.8
		C9, C10[c]	180.4	165.3
C_{20}^{2+}	I_h	C	194.7	207.3
$C_{20}H_{20}^{d}$	I_h	C	57.9	73.1 (66.9)
		H	2.4	3.4
C_{24}	D_6	C1	169.7	164.2
		C2	139.0	116.5
$C_{24}H_{12}$	D_{6d}	C1	171.2	168.7
		C2	58.8	74.2
		H	3.5	4.2
$C_6B_9N_9$	C_3	B1	35.7	33.2
		N2	114.7	140.8
		B3	41.6	29.1
		N4	236.3	248.6
		B5	46.2	41.9
		N6	189.0	207.4
		C7	241.2	215.0
		C8	121.3	132.2
C_{28}^{4-}	T_d	C1	144.7	147.2
		C2	235.5	214.0
		C3	162.0	161.1
$C_{24}N_4$	T_d	N	234.6	240.6
		C2	212.9	199.9
		C3	172.0	167.0
$C_{24}B_4$	T_d	B	47.4	45.2
		C2	140.4	140.7
		C3	222.5	220.4
$C_{24}P_4$	T_d	P	436.2	489.0
		C2	208.4	213.8
		C3	201.5	198.8
$C_{28}H_4$	T_d	C1	65.5	80.3
		C2	196.7	192.9
		C3	202.3	199.1
		H	4.1	4.7
C_{32}	D_3	C1	222.1	201.1
		C2	180.5	172.8
		C3	188.2	181.2
		C4	162.9	163.1
		C5	155.0	149.4
		C6	161.1	159.8
$C_{32}H_2$	D_3	C1	61.2	77.3
		C2	200.5	198.5
		C3	170.4	168.3
		C4	175.8	174.0
		C5	168.0	158.6
		C6	176.4	172.2
		H	3.5	3.9
C_{36}	D_{6h}	C1	142.0	137.9
		C2	155.8	155.8
		C3	162.7	158.1
C_{36}	D_{2d}	C1	153.5	149.1
		C2	154.6	155.5
		C3	160.5	152.0
		C4	143.5	138.8
		C5	143.5	138.4
C_{36}	C_{2v}	C1	93.9	66.1
		C2	151.8	139.9
		C3	185.3	180.5
		C4	166.5	164.1
		C5	165.8	159.5
		C6	155.0	151.1
		C7	165.1	158.9
		C8	151.1	154.0

Table 2. (Contd.)

Species	Symmetry	Atom	Hartree–Fock[a]	B3LYP[b]
		C9	147.8	143.8
		C10	151.2	144.0
		C11	143.5	128.2
C_{40}	D_2	C1	152.3	145.2
		C2	146.3	139.3
		C3	148.6	140.8
		C4	144.8	140.5
		C5	148.3	145.4
		C6	157.6	155.1
		C7	152.9	149.0
		C8	148.0	140.8
		C9	141.1	132.2
		C10	150.0	144.2
C_{40}	D_{5d}	C1	146.3	140.6
		C2	156.0	149.6
		C3	156.7	154.5
C_{40}^{4-}	T_d	C1	211.3	206.1
		C2	192.4	180.5
		C3	162.4	155.5
$C_{36}N_4$	T_d	N	237.3	255.0
		C2	190.9	183.2
		C3	154.7	149.8
$C_{36}B_4$	T_d	B	15.6[e]	−47.7[e]
		C2	168.6	167.0
		C3	165.1	194.2
$C_{36}P_4$	T_d	P	380.0	419.6
		C2	218.2	215.2
		C3	157.9	157.8
$C_{40}H_4$	T_d	C1	55.5	67.9
		C2	193.9	190.6
		C3	157.4	155.1
		H	4.9	5.4
C_{50}	D_{5h}	C1	148.9	146.5
		C2	160.3	164.4
		C3	159.2	160.2
		C4	144.1	116.2

[a] At GIAO-HF/6-31G*//B3LYP/6-31G*
[b] At GIAO-B3LYP/6-31G*//B3LYP/6-31G*
[c] Pairwise identical, even though not required by symmetry
[d] Experimental ^{13}C data are given in parentheses and are taken from Ref. [89]
[e] The noticeable discrepancy between Hartree–Fock and B3LYP levels for the ^{11}B chemical shift in $C_{36}B_4$ may be caused by the significantly narrower frontier orbital energy gap obtained at the B3LYP level

Table 3. Nucleus-independent chemical shift (*NICS*) values (parts per million) for the D_{6h} singlet state of C_{36} (DZP//RI-MP2/6-31G* level)

	GIAO-SCF	GIAO-BPW91	GIAO-B3LYP	GIAO-MP2
NICS (cage endo)	−35.5	−20.4	−23.7	−23.9
NICS (pentagon)	−5.4	−0.5	−1.4	−3.2
NICS (hexagon, up or down)	−23.6	−18.4	−19.5	−20.2
NICS (hexagon, equatorial)	−12.6	−4.5	−6.3	−6.7

The significance of these results is somewhat limited by the triplet instability of the lowest restricted HF (RHF) singlet wavefunction. In addition, there is an excited singlet state of the same symmetry ($^1A_{1g}$, arising from double excitation from the b_{2u} HOMO into the b_{1g} LUMO), which is only 16.6 kcal/mol higher in energy at the RHF/DZP level. According to a (6, 6) complete-active-space–SCF calculation, the corresponding configuration contributes as much as 36% to the ground-state wavefunction (DZP basis and RI-MP2 geometry). Clearly, a multiconfigurational ansatz would be required for more conclusive chemical shifts for D_{6h} C_{36}.

The NICS values computed at the B3LYP/6-31G* level are given along with those at the HF/6-31G* level in Figs. 1–7. In all cases, the antiaromatic character increases at the DFT level. However, it is interesting to note that for the species with relatively bigger HOMO–LUMO gaps, such as $C_{20}H_{20}$ and C_{28}^{4-}, the discrepancies are somewhat smaller both at the ring centers and at the cage centers. In contrast, SCF and DFT NICS values are very disparate when the HOMO–LUMO gap energies

are small. When the HOMO and LUMO become quasidegenerate at the DFT level, as is the case for $C_{36}B_4$, the B3LYP data should be regarded with caution [see, for instance, the unusual effect on $\delta(^{11}B)$ of $C_{36}B_4$, Table 2]. Unfortunately, no clear-cut trend is visible for all the species studied and further theoretical work is desirable in this direction [88].

4 Conclusion

We have presented a computational study of the smaller fullerenes C_{20}–C_{50}, selected doped analogues and hydrogen adducts, at a uniform theoretical level. Employing the GIAO approach, NMR spectra were evaluated at both the HF/6-31G* and the B3LYP/6-31G* levels of theory. Special attention was drawn to the endohedral chemical shift, which is not only a useful index for aromaticity, but also a promising characterization method for the species studied here since this endohedral shift can be accessed experimentally by the $\delta(^3He)$ value of endohedral helium compounds. The calculated NMR spectra and the endohedral helium chemical shifts for these species may be helpful for their identification. The interaction between endohedral helium and the cage, as expected, decreases strongly with increasing cage size. Once implanted into the smaller fullerenes, an endohedral helium atom should remain trapped.

Acknowledgements. This work was supported by the Deutsche Forschungsgemeinschaft (DFG). We thank the Alexander von Humboldt Foundation (Z.C.) and the Centre National de la Recherche Scientifique (H.J.) for research fellowships. M.B. thanks the DFG for a Heisenberg fellowship.

References

1. Piskoti C, Yarger J, Zettl A (1998) Nature 393: 771
2. Prinzbach H, Weiler A, Landenberger P, Wahl E, Wörth J, Scott LT, Gelmont M, Olevano D, Issendorff BV (2000) Nature 407: 60
3. Helden GV, Gotts NG, Bowers MT (1993) Nature 363: 60
4. Hunter J, Fye J, Jarrold MF (1993) Science 260: 784
5. Yang S, Taylor KJ, Craycraft MJ, Conceicao J, Pettiette CL, Cheshnovsky O, Smalley RE (1988) Chem Phys Lett 144: 431
6. Raghavachari K, Binkley JS (1987) J Chem Phys 87: 2192
7. Liang C, Schaefer HF III (1990) J Phys Chem 93: 8844
8. Pitzer KS, Clementi E (1959) J Am Chem Soc. 81: 4477
9. Sokolova S, Lüchow A, Anderson JB (2000) Chem Phys Lett 323: 229
10. Helden GV, Hsu MT, Gotts NG, Kemper PR, Bowers MT (1993) Chem Phys Lett 204: 15
11. Raghavachari K, Zhang B, Pople JA, Johnson BG, Gill PMW (1994) Chem Phys Lett 220: 385
12. Jensen F, Toftlund H (1993) Chem Phys Lett 201: 89
13. Martin JML, El-Yazal J, Francois JP (1996) Chem Phys Lett 255: 7
14. Feyereisen M, Gutowski M, Simons J, Almlöf J (1992) J Chem Phys 96: 2926
15. Jensen F, Koch H (1998) J Chem Phys 108: 3213
16. Kroto HW (1987) Nature 329: 529
17. Guo T, Diener MD, Chai Y, Alford MJ, Haufler RE, McClure SM, Ohno T, Weaver JH, Scuseria GE, Smalley RE (1992) Science 257: 1661
18. Martin JML (1996) Chem Phys Lett 255: 1
19. Portmann S, Galbraith JM, Schaefer HF III, Scuseria GE, Lüthi HP (1999) Chem Phys Lett 301: 98
20. Guo T, Smalley RE, Scuseria GE (1993) J Chem Phys 99: 352
21. Kietzmann H, Rochow R, Ganteför G, Eberhardt W, Vietze K, Seifert G, Fowler PW (1998) Phys Rev Lett 81: 5378
22. Kroto HW, Walton DRM (1993) Chem Phys Lett 214: 353
23. Lin M, Chiu YN, Xiao J (1999) J Mol Struct (THEOCHEM) 489: 109
24. Collins PG, Grossman JC, Cote M, Ishigami M, Piskoti C, Louie SG, Cohen ML, Zettl A (1999) Phys Rev Lett 82: 165
25. Koshio A, Inakuma M, Sugai T, Shinohara H (2000) J Am Chem Soc 122: 398
26. Koshio A, Inakuma M, Wang ZW, Sugai T, Shinohara H (2000) J Phys Chem B 104: 7908
27. Grossman JC, Cote M, Louie SG, Cohen ML (1998) Chem Phys Lett 284: 344
28. Cote M, Grossman JC, Cohen ML, Louie SG (1998) Phys Rev Lett 81: 697
29. Halac E, Burgos E, Bonadeo H (1999) Chem Phys Lett 299: 64
30. Slanina Z, Zhao X, Osawa E (1998) Chem Phys Lett 290: 311
31. Jagadeesh MN, Chandrasekhar J (1999) Chem Phys Lett 305: 298
32. Fowler PW, Heine T, Rogers KM, Sandall JPB, Seifert G, Zerbetto F (1999) Chem Phys Lett 300: 369
33. Fowler PW, Mitchell D, Zerbetto F (1999) J Am Chem Soc 121: 3218
34. Heine T, Fowler PW, Rogers K, Seifert G (1999) J Chem Soc Perkin Trans 2 707
35. Heine T, Fowler PW, Seifert G (1999) Solid State Commun 111: 19
36. Jishi RA, Dresselhaus MS (1999) Chem Phys Lett 302: 533
37. Yuan LF, Yang J, Deng K, Zhu QS (2000) J Phys Chem A 104: 6666
38. Chen Z, Jiao H, Hirsch A, Thiel W (2000) Chem Phys Lett 329: 47
39. Albertazzi E, Domene C, Fowler PW, Heine T, Seifert C, Alsenoy CV, Zerbetto F (1999) Phys Chem Chem Phys 1: 2913
40. Xiao J, Lin M, Chiu YN, Fu M, Lai ST, Li NN (1998) J Mol Struct (THEOCHEM) 428: 149
41. Salcedo R, Sansores LF (1998) J Mol Struct (THEOCHEM) 422: 245
42. Cui M, Zhang H, Ge M, Feng J, Tian W, Sun C (1999) Chem Phys Lett 309: 344
43. Bühl M, Thiel W (1995) Chem Phys Lett 233: 585
44. Bühl M (1998) Chem Eur J 4: 734
45. Gill PMW, Johnson BG, Pople JA, Frisch MJ (1992) Chem Phys Lett 197: 499
46. Zhong SJ, Liu CW (1997) J Mol Struct (THEOCHEM) 392: 125
47. Fowler PW, Austin SJ, Sandall JP (1993) J Chem Soc Perkin Trans 2 795
48. Choho K, Van de Woude G, Van Lier G, Geerlings P (1997) J Mol Struct (THEOCHEM) 417: 265
49. Milani C, Giambelli C, Roman HE, Alasia F, Benedek G, Broglia RA, Sanguinetti S, Yabana K (1996) Chem Phys Lett 258: 554
50. Fowler PW, Heine T, Troisi A (1999) Chem Phys Lett 312: 77
51. Kaxiras E, Jackson K, Pederson MR (1994) Chem Phys Lett 225: 448
52. Wang BC, Yu LJ, Wang WJ (1996) Int J Quantum Chem 57: 465
53. Sun KC, Chen C (1996) J Mol Struct (THEOCHEM) 360: 157
54. Strout DL (2000) J Phys Chem A 104: 3364
55. Bühl M, Thiel W, Jiao H, Schleyer, PvR, Saunders M, Anet FAL (1994) J Am Chem Soc 116: 6005
56. Bühl M, van Wüllen C (1995) Chem Phys Lett 247: 63
57. Heine T, Seifert G, Fowler PW, Zerbetto F (1999) J Phys Chem A 103: 8738
58. Sun G, Kertesz M (2000) J Phys Chem A 104: 7398
59. Sun G, Kertesz M (2000) Chem Phys Lett 328: 387
60. Sun G, Kertesz M (2000) New J Chem 24: 741

61. Heine T, Bühl M, Fowler PW, Seifert G (2000) Chem Phys Lett 316: 373
62. Schleyer PvR, Maerker C, Dransfeld A, Jiao H, Hommes NJRvE (1996) J Am Chem Soc 118: 6317
63. Saunders M, Jimenez-Vazquez HA, Cross RJ, Mroczkowski S, Freedberg DL, Anet FAL (1994) Nature 367: 256
64. Bühl M, Hirsch A (2001) Chem Rev 101: 1153
65. Becke AD (1993) J Chem Phys 98: 5648
66. Frisch MJ, Trucks GW, Schlegel HB, Scuseria GE, Robb MA, Cheeseman JR, Zakrzewski VG, Montgomery JA, Stratman RE, Burant JC, Dapprich S, Millam JM, Daniels AD, Kudin KN, Strain MC, Farkas O, Tomasi J, Barone V, Cossi M, Cammi R, Mennucci B, Pomelli C, Adamo C, Clifford S, Ochterski J, Petersson GA, Ayala PY, Cui Q, Morokuma K, Malick DK, Rabuck AD, Raghavachari K, Foresman JB, Cioslowski J, Ortiz JV, Baboul AG, Stefanov BB, Liu C, Liashenko A, Piskorz P, Komaromi I, Gomperts R, Martin RL, Fox DJ, Keith T, Al-Laham MA, Peng CY, Nanayakkara A, Gonzalez C, Challacombe M, Gill PMW, Johnson BG, Chen W, Wong MW, Andres JL, Gonzales C, Head-Gordon M, Replogle ES, Pople JA (1998) Gaussian 98. Gaussian, Pittsburgh, Pa
67. Jameson CJ, Dedios A, Jameson AK (1990) Chem Phys Lett 167: 575
68. Bühl M, Schleyer PvR (1992) J Am Chem Soc 114: 477
69. Gauss J (1993) J Chem Phys 99: 3629
70. Kollwitz M, Gauss, J (1996) Chem Phys Lett 260: 639
71. Huzinaga S (1971) Approximate atomic wave functions. University of Alberta, Edmonton
72. Weigend F, Häser M (1997) Theor Chem Acc 97: 331
73. Eichkorn K, Weigend F, Treutler O, Ahlrichs R (1997) Theor Chem Acc 97: 119
74. Weigend F, Haser M, Patzelt H, Ahlrichs R (1998) Chem Phys Lett 294: 143
75. Ahlrichs R, Bär M, Häser M, Horn H, Kölmel M (1989) Chem Phys Lett 154: 165
76. Becke AD (1988) Phys Rev A 38: 3098
77. Perdew JP (1991) In: Ziesche P, Eschrig H (eds) Electronic structure of solids. Akademie, Berlin, p 11
78. Perdew JP, Wang Y (1992) Phys Rev B 45: 13244
79. Hirsch A, Chen Z, Jiao H (2000) Angew Chem Int Ed Engl 39: 3915
80. Fokin AA, Jiao H, Schleyer PvR (1998) J Am Chem Soc 120: 9364
81. Schleyer PvR, Jiao H, Hommes NJRvE, Malkin VG, Malkina OL (1997) J Am Chem Soc 119: 12669
82. Fan MF, Lin Z, Yang S (1995) J Mol Struct (THEOCHEM) 337: 231
83. Jagadeesh MN, Makur A, Chandrasekhar J (2000) J Mol Model 6: 226
84. Cross RJ, Saunders M, Prinzbach H (1999) Org Lett 1: 1480
85. Jimenez-Vazquez HA, Tamariz J, Cross RJ (2001) J Phys Chem A 105: 1315
86. Shriver DF, Atkins PW, Langford CH (1994) Inorganic chemistry, 2nd edn. Oxford University Press, Oxford, p 59
87. Bühl M, Patchkovskii S, Thiel W (1997) Chem Phys Lett 275: 14
88. Bühl M, Kaupp M, Malkina OL, Malkin VG (1999) J Comput Chem 20: 91
89. Breitmaier E, Voelter W (1987) Carbon-13 NMR spectroscopy, 3rd edn. VCH, Weinheim